

Light-controlled pulsed x-ray tube with photocathode

Hao Xuan(宣浩), Yong-An Liu(刘永安), Peng-Fei Qiang(强鹏飞), Tong Su(苏桐), Xiang-Hui Yang(杨向辉), Li-Zhi Sheng(盛立志), and Bao-Sheng Zhao(赵宝升)

Citation: Chin. Phys. B, 2021, 30 (**11**): 118502. DOI: 10.1088/1674-1056/abff1e
Journal homepage: http://cpb.iphy.ac.cn; http://iopscience.iop.org/cpb

What follows is a list of articles you may be interested in

Realizing photomultiplication-type organic photodetectors based on C_{60}-doped bulk heterojunction structure at low bias

Wei Gong(龚伟), Tao An(安涛), Xinying Liu(刘欣颖), Gang Lu(卢刚)
Chin. Phys. B, 2019, 28 (**3**): 038501. DOI: 10.1088/1674-1056/28/3/038501

A theoretical and experimental evaluation of III-nitride solar-blind UV photocathode

Bin Ren(任彬), Hui Guo(郭晖), Feng Shi(石峰), Hong-Chang Cheng(程宏昌), Hui Liu(刘晖), Jian Liu(刘健), Zhi-Hui Shen(申志辉), Yan-Li Shi(史衍丽), Pei Liu(刘培)
Chin. Phys. B, 2017, 26 (**8**): 088504. DOI: 10.1088/1674-1056/26/8/088504

Comparison of blue-green response between transmission-mode GaAsP-and GaAs-based photocathodes grown by molecular beam epitaxy

Gang-Cheng Jiao(焦岗成), Zheng-Tang Liu(刘正堂), Hui Guo(郭晖), Yi-Jun Zhang(张益军)
Chin. Phys. B, 2016, 25 (**4**): 048505. DOI: 10.1088/1674-1056/25/4/048505

Preliminary results for the design, fabrication, and performance of a backside-illuminated avalanche drift detector

Qiao Yun, Liang Kun, Chen Wen-Fei, Han De-Jun
Chin. Phys. B, 2013, 22 (**10**): 108504. DOI: 10.1088/1674-1056/22/10/108504

Light-controlled pulsed x-ray tube with photocathode*

Hao Xuan(宣浩)[1,2], Yong-An Liu(刘永安)[1], Peng-Fei Qiang(强鹏飞)[1], Tong Su(苏桐)[1], Xiang-Hui Yang(杨向辉)[1], Li-Zhi Sheng(盛立志)[1,†], and Bao-Sheng Zhao(赵宝升)[1]

[1] *State Key Laboratory of Transient Optics and Photonics, Xi'an Institute of Optics and Precision Mechanics, Chinese Academy of Sciences (CAS), Xi'an* 710119, *China*

[2] *University of Chinese Academy of Sciences, Beijing* 100049, *China*

(Received 18 January 2021; revised manuscript received 8 April 2021; accepted manuscript online 8 May 2021)

Unstable mechanical structure, low energy efficiency, and cooling requirements limit the application of conventional x-ray tubes based on filament as cathode in several academic areas. In this paper, we demonstrate a light-controlled pulsed x-ray tube using multialkali cathode as electron generator. The photocathode active area of the light controlled x-ray tube is 13.2 cm^2 (41 mm in diameter), which provides high photoelectron-emitting efficiency up to 0.288 mA/lm in 460-nm LED and 2.37-mA maximum tube current. Furthermore, the modulation ability from 1 kHz to 100 kHz of the x-ray tube is tested. The results suggest that the light-controlled pulsed x-ray tube has easy modulation and short x-ray pulse properties and is promising to be the next generation x-ray tube with wide applications in medical radiation therapy as well as the calibration for detectors and scintillators.

Keywords: x-ray source, photocathode, x-ray modulation

PACS: 85.45.Bz, 85.60.Ha, 98.70.Qy **DOI:** 10.1088/1674-1056/abff1e

1. Introduction

As the key component for x-ray application in security inspection and medical radiation therapy,[1–3] high energy, high tube current, and easy-maintained x-ray tube has been a hotspot for decades. The traditional x-ray tube is based on thermionic cathode with filament to generate electrons since the discovery of x-rays.[4] Electrons from the heated tungsten filament are accelerated and bombard the anode target to produce x-rays.[5] However, life of the thermionic cathode is limited because the filament gets thinner and thinner through the sublimation of the oxides while it is heating. Accordingly, heat brought by low-energy-efficiency filament requires much consideration to design the appropriate heat-dissipation structure. In addition, a major problem with the application of thermionic cathode is it is hard to adjust the output x-ray intensity rapidly. A grid-control structure is used to modulate the intensity of output x-rays within the thermionic-cathode-based x-ray tube in the x-ray communication system.[6–8] Output x-ray intensity cannot be modulated in high speed since the amplitude of the grid voltage is relatively too large to change rapidly in the nanosecond scale which restricts the performance of x-ray communication system.[7] Therefore, it is crucial to find advanced methods to replace thermionic cathode with better performance, thermal stability, and easy modulation access.

Several new cathodes have been proposed and developed, such as cold cathode based on metal or carbon nanotube,[9–13] laser-plasma x-ray generation,[14,15] and free-electron laser.[16–18] However, detaching from the substrate for carbon nanotubes and high cost, large volumes of laser are still unsolved problems that limit their application to some extent. Another method that used photocathode to generate x-rays was reported by the company Hamamatsu Photonics in 1992.[19] A modulated laser and photocathode were used to achieve 50-μA tube current and maximum energy of x-rays to 30 keV. Relative research to improve tube current to 1 mA was proposed by Timofeev adopting dynode system in 2018.[20,21] But the spark caused by dynode and high anode voltage might have fatal damage to the performance of the x-ray tube.

In this paper, photocathode with S20 multialkali material and LED in the 460-nm wavelength were used to design a high-tube-current and easy-modulated x-ray tube. In the case of the high quantum efficiency of S20 cathode, 2.37-mA high-tubecurrent and maximum energy up to 25 keV were achieved without dynode system. Meanwhile, modulation ability of this light-controlled pulsed x-ray tube was investigated and the results show this x-ray tube is expected to have the potential to achieve high tube current and better modulation ability compared with thermionic cathode.

2. Structures and experiments

The structure of the light-controlled pulsed x-ray tube is shown in Fig. 1. There are four main parts of the tube, including light source, photocathode, tungsten anode, and high voltage.

*Project supported by the National Natural Science Foundation of China (Grant Nos. 61901470 and U1931138), the Strategic Pioneer Program on Space Science, Chinese Academy of Sciences (Grant No. XDA15020501-04), the CAS "Light of West China" Program (Grant No. XAB2018A07), and the Foundation of State Key Laboratory of China (Grant No. SKLIPR2021).

†Corresponding author. E-mail: lizhi_sheng@opt.ac.cn

© 2021 Chinese Physical Society and IOP Publishing Ltd

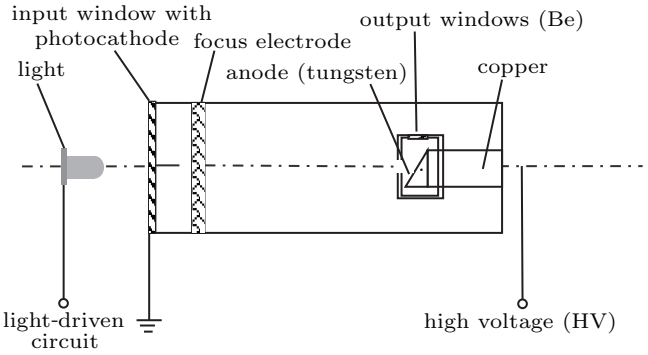


Fig. 1. Schematic diagram of the light-controlled pulsed x-ray tube. Photocathode was excited by two LEDs in 460-nm wavelength and the photoelectrons are accelerated to the anode at 25-kV voltage to generate x-rays.

2.1. Structure

2.1.1. Light source

The light source consists of two LEDs and a signal modulation circuit. Output x-ray intensity could be modulated by adjusting the power of the LEDs. Some researches have reported that the maximum modulation rate of the commercially LED could be MHz level,[22] which could satisfy the requirement in our experiment effectively. The Na_2KSb (Cs) (S20 cathode) alkali metal telluride cathode was used in this photocathode and two blue LEDs (characteristics in Table 1) with a wavelength of 460 nm were adopted to match the characteristic of the S20. The LEDs were mounted on a cylindrical, heat-dissipating aluminum block to dissipate the heat from the LEDs.

Table 1. Characteristics of LED (460 nm).

Properties	Parameters
Emission wavelength	460 nm
Rated power	3 W
Pulse repetition rate	DC to 4 MHz
Divergence angle	120°

In addition, a constant current source was adopted as the LED modulation circuit, and the On-Off-Key (OOK) modulation was used in the experiment. The status of LED was controlled by MOSFET IRF510: when the modulation signal is at high level, MOSFET turn "on", the x-ray tube works; when at low level, MOSFET turn "off", there is no x-ray photon. The illustrated circuit in Fig. 2 was used in our experiment.

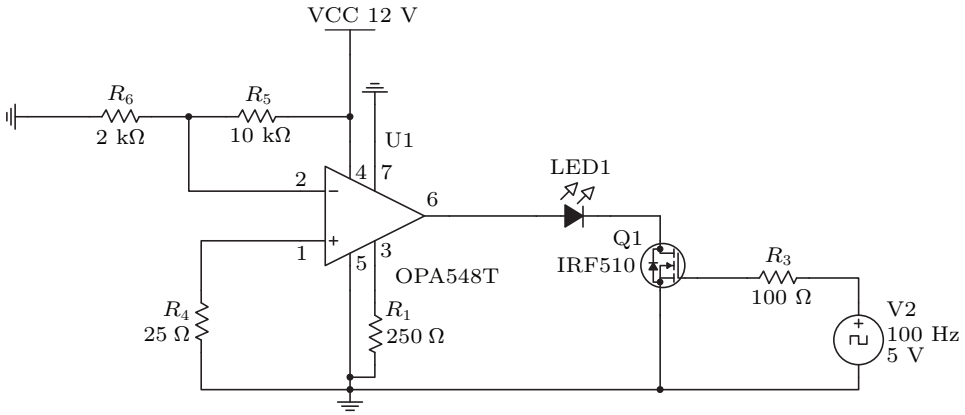


Fig. 2. LED modulation circuit with OPA548T providing maximum 400-mA current and IRF510 MOSFET to realize modulation.

2.1.2. Photocathode

By evaporating a photocathode material of sufficient thickness on a quartz glass input window (diameter 4.1 cm and thickness 0.55 cm), the photocathode with the approximately 120 nm-layer shown in Fig. 3(b) was made and used to produce photoelectrons. In the 460-nm excited-light wavelength, the thermal-evaporated S20 cathode has a quantum efficiency of up to 20%, which could generate enough photoelectrons. Photoelectric sensitivity is 0.117 mA/lm after the S20 material evaporation was completed.

The photoelectron material layer (S20) was deposited on the glass substrate by thermal evaporation, and the real-time photocurrent was monitored by the system to realize the optimal layer thickness based on cumulative experience. An ultra-high vacuum environment is required during the cathode evaporation thus the vacuum of the seal system is maintained at the level of 10^{-7} Pa. High purity potassium chromate, sodium chromate and cesium chromate in analytical standards as well as antimony particles with 99% purity are the raw materials for the photocathode layer. Firstly, the sodium layer was deposited above the quartz glass until the photocurrent monitored was found to be stable with time; secondly, antimony particles were subsequently slowly evaporated before the photocurrent decreased from 50% to 30% of the peak value; thirdly, the potassium layer was deposited until the photocurrent reached its new peak. The thickness of the photocathode layer at this time was approximately 120 nm. Finally, the layer above was exposed to the cesium steam five times to achieve stable-performance photocathode.

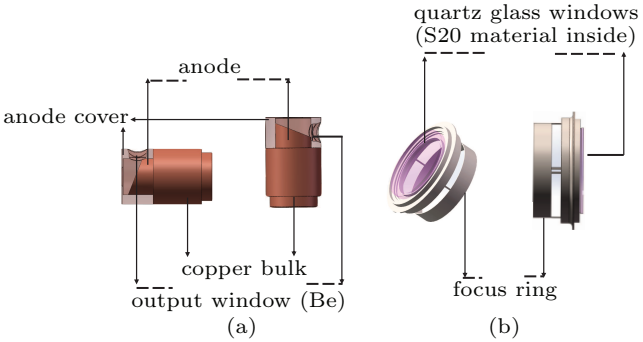


Fig. 3. Cathode and anode of the tube. (a) Reflective anode and cooper base, (b) photocathode and focus electrode.

The large bombardment area caused by the unfocused electron beam will negatively affect the quality of the output x-rays since electrons escape from the entire photocathode plane. Therefore, the focus structure is essential to reduce the bombardment area of the electron beam from the photocathode to the anode. A focus ring was used in the tube to change internal electric field which forces the electrons to move towards the central part of the anode target. According to the simulation result shown in Fig. 4(a), the electron beam was obviously focused, and a smaller bombardment area was obtained on the anode. The width of the focus ring used in this experiment is 10.0 mm based on the simulation result in Fig. 4(b), which showed that most electrons bombarded the anode in a 15.1-mm diameter circle and the effective bombardment area was approximately 114 mm^2.

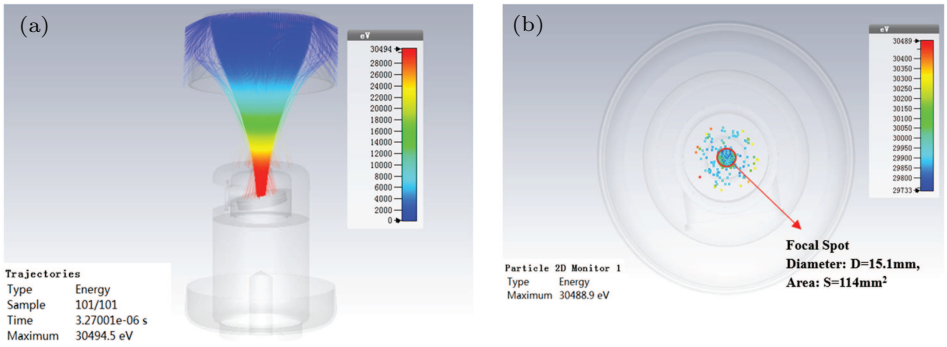


Fig. 4. (a) Simulation of electron trajectories. Compared with the photocathode-emitting plane, electrons were focused in a much smaller region. (b) The bombardment area on the anode.

2.2. Anode and high voltage

Reflective anode with tungsten (diameter 23.36 mm) and 18° inclination shown in Fig. 3(a) was adopted. The dimension of the copper cooling cylinder was 35 mm in diameter and 48 mm in height. Besides, to obtain a high-quality focused electron beam, a unique anode cover shown in Fig. 3(a) was used above the anode. An entrance with a diameter of 10.5 mm was dug out at the top of the anode cover which allows the electron to pass through, and the unfocused electrons were blocked, unable to generate x-ray photon. Besides, a 27 mm×2 mm beryllium window on the side of the cover structure allows x-ray photons to exit.

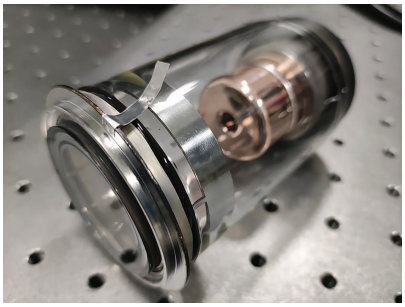


Fig. 5. Light-controlled pulsed x-ray tube with photocathode.

The anode was biased to the positive high voltage and the cathode was grounded in order to generate the high-voltage electric field in the tube. The photocathode and the focus electrode were connected via lead wires to the outside of the quartz shell. Figure 5 shows the tube we designed.

2.3. Experiments

The light-controlled pulsed x-ray tube was tested by illuminating the S20 photocathode with blue LED powered by a constant current source. Figure 6 shows the simulation about the light intensity distribution on the plane at different distances from the center of the LED light source based on the assumption that the LED source is Lambert radiator. According to Fig. 6, the distance between the LED and the photocathode was fixed at 2 cm, which could satisfy the maximum input light intensity of the photocathode, and also prevent the heat of the LED from affecting the photocathode.

Additionally, the modulation ability of the x-ray tube was also tested in the experiment. An easier x-ray modulation access could be obtained because of the properties of the photocathode and LED. Figure 7 shows the process of the modulation-test experiment, loading square wave signals of various frequencies on the LED modulation circuit shown in Fig. 2 and viewing the restored waveform through an oscilloscope.

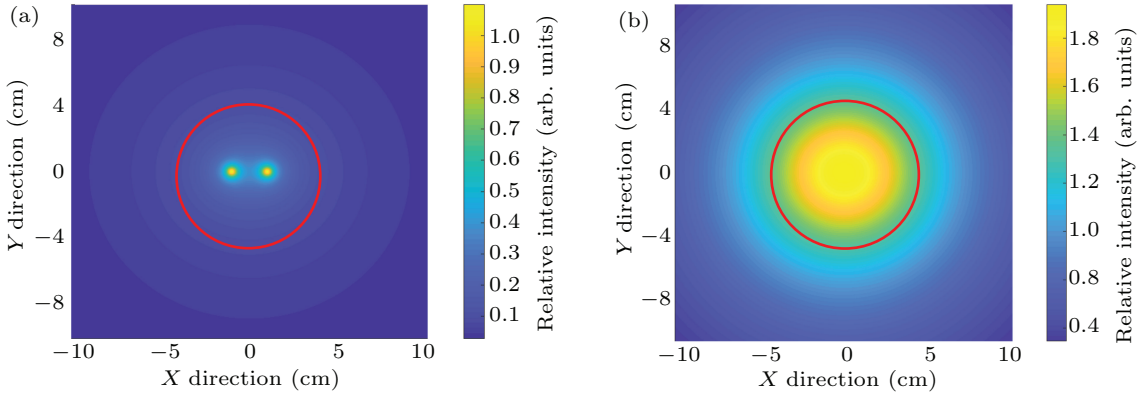


Fig. 6. Simulation on light intensity distribution at different distances in (a) 0.1 cm, (b) 2-cm, and red circle is the photocathode plane (diagram 4.10 cm).

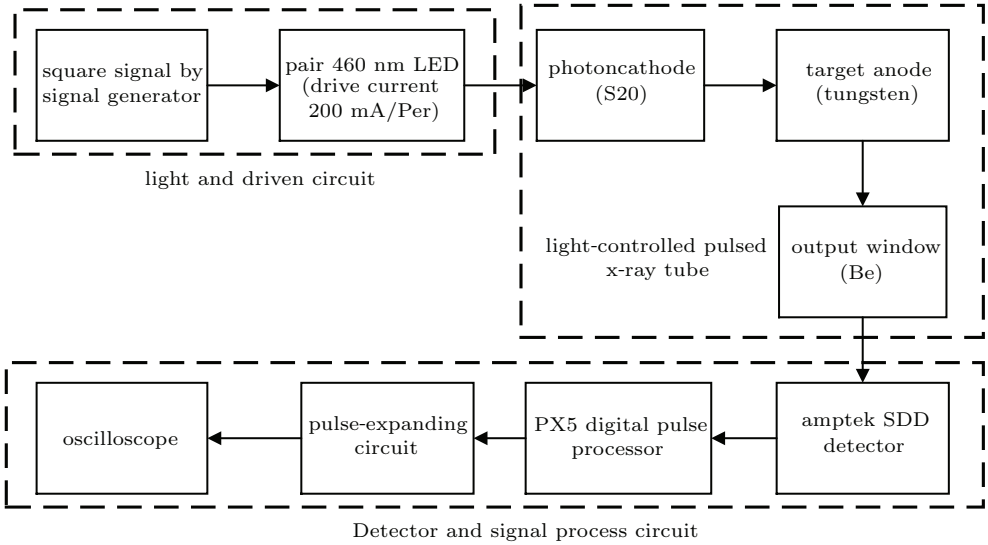


Fig. 7. Schematic diagram of the experiment to the modulation ability of x-ray tube.

3. Result and discussion

3.1. Measurement of tube current

Relationship between anode voltage and x-ray tube current was investigated when the LED power was fixed at 0.130 W, 0.256 W, 0.381 W, 0.556 W, 0.710 W, and 0.870 W. The anode voltage was changed from 10 kV to 25 kV. Figure 8 presents the results obtained from the experiments above.

Results in Fig. 8 show that x-ray tube current remained constant while the anode voltage was changed, which indicated that there was no apparent relation between the tube current and the anode voltage of 10 kV–25 kV for light-controlled pulsed x-ray tube. The tube current remained stable in fixed LED power if the anode voltage higher than a "threshold" to generate x-ray photon. That property is quite different from thermionic cathode x-ray tube. Light intensity and photocathode material should be paid more attention to because anode voltage was not an important factor having a great effect on the x-ray tube performance in contrast to the thermionic-based x-ray tube.

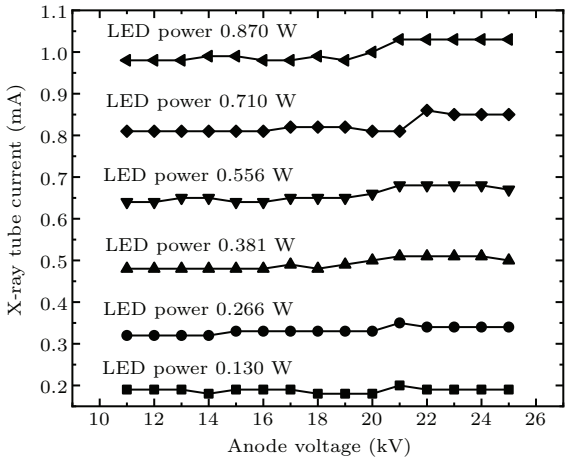


Fig. 8. X-ray tube current remains relatively stable under different anode high voltage with fixed LED power.

Based on the above conclusions, the effect of anode voltage could be overlooked when we measured the relation between LED power and tube current. The relationship between LED power and tube current was measured with 2-cm distance from LED to photocathode and 10-kV anode-voltage. The experimental results introduced in Fig. 9 showed that the rapid

rise of tube current was consistent with the increment of the LED power because of more photoelectrons on the photocathode.

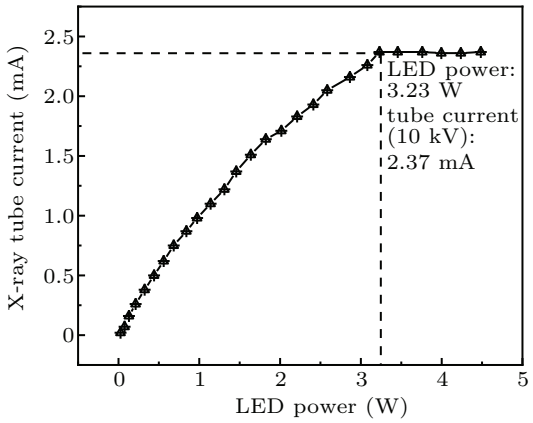


Fig. 9. The increase of tube current associated with LED power and the saturation tube current is 2.37 mA, while the LED power is 3.23 W.

As can be seen from Fig. 9, the x-ray tube current increased linearly with the LED power before the number of photoelectrons was not yet saturated. When the LED power increased to 3.23 W, the maximum value of tube current was 2.37 mA with a current emission density of 0.178 mA/cm^2 and an efficiency of 0.238 mA/lm$\times$cm^2 (in 460 nm) for the S20 photocathode.

3.2. Measurement of modulation ability

The light-controlled pulse x-ray tube has easy access to be modulated, compared with the traditional thermionic cathode x-ray tube. The experimental theory of the modulation waveform restoration experiment is that, using the XR-100 silicon drift detector (SDD) and PX5 pulse processor developed by Amptek, when the x-ray is detected by the detector, the PX5 will generate a pulse signal. We use an external circuit to eliminate the noise signal by changing the threshold, detect the pulse signal, and convert it to a square wave signal. Assuming that there are N x-ray photons detected in an input signal cycle $T_{\rm in}$, and each pulse will be expanded to a square wave signal with a pulse width of $t_{\rm ex}$. In that case, the pulse width of the output restored waveform is $T_{\rm out} = N \times t_{\rm ex}$, where $t_{\rm ex}$ can be changed under various experimental conditions by adjusting the resistance value. The results obtained from the preliminary experiment of modulation ability are displayed in Figs. 10–12.

From the experimental results, the restored waveform was in almost perfect concordance with the input signal in the low frequency from 1 kHz to 10 kHz. x-ray photons were sufficiently numerous in each period so the expand circuit could use these pulses to restore waveform which has the same time width as the input signal.

However, different amounts of the detected photon events could be observed through the result of the oscilloscope in Fig. 11, which results in different widths of the restored waveform. The limiting factor affecting the restored signal had changed to the number of x-ray photons while modulation speeds up to 60 kHz and 70 kHz. Input rate shown by SDD detector was 17 kcps, which could not satisfy the requirement that there were enough x-ray photons in every cycle. It can be seen from the experimental results that in most cycles, there were enough x-ray photons to make $T_{\rm out} = T_{\rm in}$; but in a few periods, the number of x-ray photons was relatively small, resulting in $T_{\rm out}$ less than $T_{\rm in}$. In addition, although the photoelectron emission was instantaneous, the SDD output pulse time and the rising edge of the input signal often could not completely correspond, so there was a delay in the restored waveform.

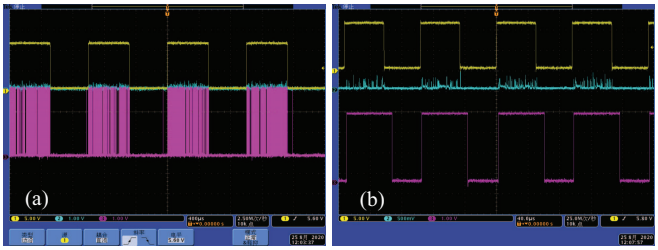


Fig. 10. Picture of input signal (yellow), SDD detector signal (blue), and restore signal (red) in (a) 1 kHz, (b) 10 kHz. The contour of the restored signal is basically the same as the contour of the input signal.

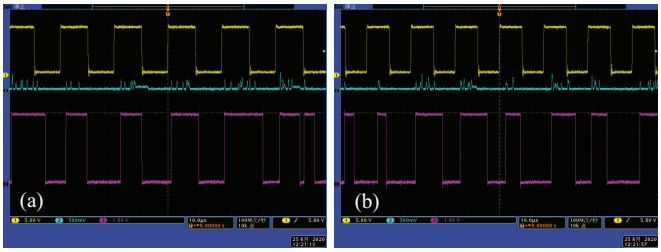


Fig. 11. Picture of input signal (yellow), SDD detector signal (blue), and restore signal (red) in (a) 60 kHz, (b)70 kHz. Owing to the restriction of the number of x-ray photons, the restored signal deviates from the input signal.

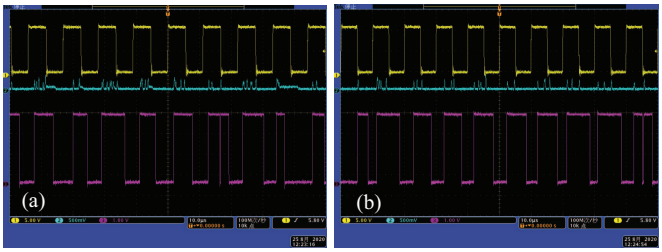


Fig. 12. Picture of input signal (yellow), SDD detector signal (blue), and restore signal (red) in (a) 90 kHz, (b) 100 kHz. The restored signal was basically the same as the input signal, but the time position was shifted.

The situation of modulation rate in 90 kHz and 100 kHz was better than 60 kHz and 70 kHz, mainly because of the short input signal duration. But the time position shift of the restored signal could be clearly observed in the case of the x-ray photon signal arrives between the pulse duration rather

than the rising edge. The distortion problem will become more serious with the further increase of the conversion frequency to the restored waveform. Therefore, more attention must be paid to the increase in the number of x-ray photons in future studies to achieve a higher modulation rate x-ray tube.

According to the above experimental conditions, the amount of the x-ray photons is the main parameter that affects the tube's modulation performance. X-ray photon number fluctuations could be neglected because of the enormous amount of detected photon signals in each cycle in the relatively low modulated frequency. But this fluctuation could be clearly observed in the high modulated frequency due to there were only less than 10 photons in each cycle. Hence, the restored waveform's distortion in high frequency is the manifestation of the x-ray photon number fluctuation. For better modulated performance, more x-ray photons are the most critical consideration.

4. Conclusion

By combing blue LEDs in 460-nm wavelength and high-quantum efficiency multialkali cathode, we have designed a light-controlled pulsed x-ray tube with the maximum 2.37-mA tube current by photocathode efficiency 0.288 mA/lm (in 460 nm). Furthermore, the studies illustrated the modulation performance of this tube in different modulating rates, which show the easy-access modulation property of the tube we design. Further research should focus on the improvement of output x-ray energy as well as the number of the emitting x-ray photons by improving the construction process and modifying the tube structure adding a beryllium window on the shell. Besides, the potential application of the light controlled pulsed x-ray tube in XCOM system and x-ray pulsar navigation ground experiment system will be investigated as well.

References

[1] Miao C, Xie L, Wan F, Su C, Liu H, Jiao J and Ye Q 2019 *Proceedings of the IEEE Conference on Computer Vision and Pattern Recognition*, June 16–20, Long Beach, USA, p. 2119

[2] Baskar R, Lee K A, Yeo R and Yeoh K W 2012 *Int. J. Med. Sci.* **9** 193

[3] Grotzer M, Schültke E, Bräuer-Krisch E and Laissue J 2015 *Physica Medica* **31** 564

[4] Glasser O 1993 *Wilhelm Conrad Rontgen and the early history of the Roentgen rays* (San Francisco: Norman Publishing) pp. 1–15

[5] Merzbacher E and Lewis H 1958 *Corpuscles and Radiation in Matter II/Korpuskeln und Strahlung in Materie II* (Berlin: Springer) pp. 166–192

[6] Zhao B, Yan Q, Sheng L and Liu Y (Chinese Patents) CN103077874 [2011-10-25]

[7] Wang L Q, Su T, Zhao B S, Sheng L Z, Liu Y A and Liu D 2015 *Acta Phys. Sin.* **64** 120701 (in Chinese)

[8] Su T, Tang L, Li Y, Sheng L and Zhao B 2019 *Optik* **199** 163263

[9] Dyke W, Dolan W 1956 *Advances in electronics and electron physics* (Elsevier) pp. 89–185

[10] Sugie H, Tanemura M, Filip V, Iwata K, Takahashi K and Okuyama F 2001 *Appl. Phys. Lett.* **78** 2578

[11] Qian X, Tucker A, Gidcumb E, Shan J, Yang G, Calderon-Colon X, Sultana S, Lu J, Zhou O and Spronk D 2012 *Medical Physics* **39** 2090

[12] Lei W, Zhu Z, Liu C, Zhang X, Wang B and Nathan A 2015 *Carbon* **94** 687

[13] Heo S H, Ihsan A and Cho S O 2007 *Appl. Phys. Lett.* **90** 183109

[14] Tsai H E, Wang X, Shaw J M, Li Z, Arefiev A V, Zhang X, Zgadzaj R, Henderson W, Khudik V and Shvets G 2015 *Phys. Plasmas* **22** 023106

[15] Andriyash I, Lehe R, Lifschitz A, Thaury C, Rax J M, Krushelnick K and Malka V 2014 *Nat. Commun.* **5** 1

[16] Ishikawa T, Aoyagi H, Asaka T, Asano Y, Azumi N, Bizen T, Ego H, Fukami K, Fukui T and Furukawa Y 2012 *Nat. Photon.* **6** 540

[17] Vinko S, Ciricosta O, Cho B, Engelhorn K, Chung H-K, Brown C, Burian T, Chalupsky J, Falcone R and Graves C 2012 *Nature* **482** 59

[18] Amann J, Berg W, Blank V, Decker F J, Ding Y, Emma P, Feng Y, Frisch J, Fritz D and Hastings J 2012 *Nat. Photon.* **6** 693

[19] Derenzo S, Moses W, Blankespoor S, Ito M and Oba K *IEEE Conference on Nuclear Science Symposium and Medical Imaging*, October 26–31, 1992, Orlando, USA, pp. 117–119

[20] Timofeev G, Potrakhov N, Nechaev A 2019 *AIP Conf. Proc.* Volume 2089

[21] Timofeev G and Potrakhov N 2018 *25th International Conference on Vacuum Technique and Technology*, June 5–7, 2018, St. Petersburg, Rassian Federation, Volume 387

[22] Grubor J, Lee S C J, Langer K D, Koonen T and Walewski J W 2007 *33rd European Conference and Exhibition of Optical Communication*, September 16–20, Berlin, Germany pp. 1–2